Response of Jupiter's UV auroras to interplanetary conditions as observed by the Hubble Space Telescope during the Cassini fly-by campaign

J.D. Nichols*[1], E.J. Bunce[1], J.T. Clarke[2], S.W.H. Cowley[1], J.-C. Gérard[3], D. Grodent[3], and W.R. Pryor[4]

1 Department of Physics & Astronomy, University of Leicester, Leicester LE1 7RH, UK
2 Center for Space Physics, Boston University, Boston, MA 02215, USA
3 LPAP, Institut d'Astrophysique et de Géophysique, Université de Liège, B-4000 Liège, Belgium
4 Central Arizona College, 8470 N. Overfield Road, Coolidge, AZ 85228, USA

Draft A: Submitted to *Journal of Geophysical Research*, August 2006

*Corresponding author:
Tel.: 0044 116 252 5049; Fax: 0044 116 252 3555; E-mail: jdn@ion.le.ac.uk

Abstract.

We provide a first detailed discussion of the relation between the set of jovian UV auroral images observed by the Hubble Space Telescope (HST) in Dec 2000-Jan 2001 and simultaneous interplanetary data obtained by Cassini during its Jupiter fly-by. Examination of the interplanetary data surrounding all seven HST observation intervals shows that by chance six of them correspond to solar wind rarefaction regions, which follow compressions by periods of ~2 to ~6 days. Only one imaging interval, on 13 Jan 2001, corresponds to a compression region of generally elevated, but highly variable, solar wind dynamic pressure and interplanetary field strength. We have thus first examined the images corresponding to rarefaction regions in order to establish the range of behaviours that occur under these known conditions, which then act as a benchmark against which the compression region images can be compared. The rarefaction region images show relatively consistent properties of the main oval auroras, though differing in detail from interval to interval. The polar auroras show more variability, with the patchy ('swirl') auroras in the central region sometimes forming a diffuse ring structure and at other times being more uniformly distributed, while the 'active region' auroras at dusk vary markedly from weak emissions to bright arc-like forms, the latter possibly being associated with intervals within ~2-3 days of a previous solar wind compression. The two images obtained in the compression region on 13 Jan 2001 then show remarkably different properties in all the auroral components. The main oval is found to be brighter over its whole length by factors of two to three compared with the rarefaction region images, while its position remains essentially unchanged, close to the usual reference oval. However, bright contiguous 'active region' auroras in the post-noon and dusk sector then widen the overall auroral distribution in that sector by up to ~5° in the poleward direction. The region of patchy polar auroras is also found to expand to cover essentially the whole of the remaining area of the polar cap, with a much-narrowed darker zone just poleward of the main oval in the dawn and pre-noon sector. We discuss whether these enhanced emissions are characteristic of the few-day compression region as a whole, or of more localised conditions occurring within the compression region, and conclude that the latter is more likely. Examination of the relevant interplanetary data then shows that the brightened images are associated with an interval of significant magnetospheric dynamics, involving a modest compression of the magnetosphere followed by an extended major expansion.

Key words. Magnetospheric physics (Auroral phenomena, planetary magnetospheres, solar wind-magnetosphere interactions)

1. Introduction

This paper is concerned with Jupiter's ultraviolet (UV) auroras and their response to the interplanetary medium, as observed by the Hubble Space Telescope (HST) during the flyby by the Cassini spacecraft in Dec 2000 – Jan 2001. These auroras consist of three distinct components, each of which should behave in differing ways. With increasing latitude these are the moon footprints, the main auroral oval, and the highly variable 'polar auroras' poleward of the main oval. The moon footprints are associated with flux tubes that map to the equatorial plane deep within the magnetosphere, e.g. to Io's orbit at ~6 R_J. These auroras are not, therefore, expected to be controlled significantly by conditions in the interplanetary medium. The main auroral oval, which is believed to be due to the region of upward field-aligned current associated with the breakdown of corotation of outwardly-diffusing iogenic plasma, maps to the equatorial plane in the middle magnetosphere between ~20 and ~40 R_J [*Cowley and Bunce,* 2001*; Hill* 2001*; Khurana,* 2001*; Southwood and Kivelson,* 2001*; Nichols and Cowley,* 2004]. Theoretical considerations have suggested that the intensity of the main oval should be anti-correlated with the dynamic pressure of the solar wind [*Southwood and Kivelson,* 2001*; Cowley and Bunce,* 2001, 2003a,b]. For example, if the dynamic pressure decreases the magnetosphere expands and the angular velocity of the equatorial plasma reduces, thus increasing the magnitude of the magnetosphere-ionosphere coupling currents and the associated auroral emission. Conversely, if the dynamic pressure of the solar wind increases the magnetosphere contracts, the plasma angular velocity increases, and the coupling currents and auroras are reduced. It has also been suggested, however, that under conditions of sufficiently strong compression the coupling current system could in principle reverse in sense if plasma super-rotation is induced relative to the neutral atmosphere [*Cowley and Bunce*, 2003a,b], an effect that may be temporarily enhanced by atmospheric inertia [*Gong and Hill*, 2005]. In this case the 'main oval' aurora will form poleward of the usual location, while the latter region will become aurorally dark, associated with downward field-aligned currents.

The polar auroras map to the outer parts of the magnetosphere and may thus be expected to exhibit a more direct relation to the interplanetary medium, since the region will contain those field lines that map to the vicinity of the magnetopause and the open field lines of the tail lobes [*Cowley et al.,* 2003*; Stallard et al.,* 2003]. *Cowley et al.* [2005] used a simple axisymmetric model of the ionospheric plasma flow in the outer magnetosphere and open tail region to show that a ring of aurora, emitting much less power than the main oval, is expected to occur poleward of the main oval on flux tubes mapping to the open-closed field line boundary. Such secondary polar ovals have been reported in the past [*Prangé et al.,* 1998*; Pallier and Prangé,* 2001] and may be related. Equally significant is a highly variable auroral patch or spot that occurs in the noon/post-noon

sector and is occasionally observed to 'flare' from a typical brightness of a few kR to ~10 MR over brief periods. This emission has been suggested to be associated with the jovian cusp [e.g. *Clarke et al.,* 1998*; Pallier and Prangé,* 2001*; Waite et al.,* 2001*; Grodent et al.,* 2003a]. *Bunce et al*. [2004] theoretically considered the effects of pulsed dayside reconnection at Jupiter, and showed that a bi-polar (i.e. adjacent upward- and downward-directed) field-aligned current pair is produced, associated with a twin-vortical flow system that is excited across the open-closed field line boundary. They showed that for sufficiently strong reconnection pulses the region of upward current will be associated with strongly downward-accelerated magnetospheric electron fluxes that will produce bright UV auroras, while the adjacent region of downward current will be carried by downward-accelerated magnetospheric heavy ions that will produce significant X-ray emission. This pattern of adjacent UV and X-ray emission in the 'cusp' region has been confirmed by simultaneous Chandra/HST observations reported by *Elsner et al.* [2005]. With regard to the flux transport associated with these reconnection processes, *Nichols et al.* [2006] have recently shown that although the reconnection voltage at Jupiter is often negligibly small, e.g. during solar wind rarefaction conditions, such that the magnetosphere is then clearly corotation-dominated, voltages up to a few MV are often generated during the regular enhancements in the strength of the interplanetary magnetic field (IMF) that are associated with corotating interaction regions (CIRs) and coronal mass ejections (CMEs).

Past studies of the dependence of Jupiter's auroras on interplanetary conditions have been severely limited by the lack of upstream monitoring at Jupiter's orbit. However, spacecraft fly-bys provide valuable, albeit brief, periods of in situ data concerning the conditions in the nearby interplanetary medium. For example, *Baron et al.* [1996] examined Jupiter's infrared auroras (H_3^+ emission) observed by ground-based telescope during the 1992 Ulysses Jupiter fly-by, and compared overall auroral brightness with the solar wind dynamic pressure. They found the two quantities were directly correlated to a degree whereby there was less than 1% chance of them being unrelated. In Dec 2000-Jan 2001 the Cassini spacecraft performed a gravity assist manoeuvre at Jupiter, en route to Saturn, leading to a number of reports on the joint Cassini-Galileo data set [e.g. *Hanlon et al.,* 2004a,b*; Achilleos et al.,* 2004*; Svenes et al.,* 2004]. *Gurnett et al.* [2002] and *Pryor et al.* [2005] also reported Cassini observations of UV emissions and hectometric radio emissions from Jupiter in which the magnitudes increased by factors of 2-4 over several hours during intervals associated with CIR compression regions and CMEs. However, Jupiter was spatially unresolved in these UV observations such that it remains unclear as to which component of the auroras is responsible for the increased power output.

In addition to these studies, a campaign of observations of Jupiter's auroras was also undertaken during the Cassini flyby using the Space Telescope Imaging Spectrograph (STIS) onboard the HST. The resulting images have been extensively studied by *Grodent et al.* [2003a,b], both with regard to the main oval and the polar auroras. It was noted in particular that one set of images in which the main oval was particularly bright, obtained on 13 Jan 2001, was associated with an interval of increased solar wind dynamic pressure, in apparent contradiction to the simple theoretical expectation discussed above. However, a more detailed comparison of the HST images and the Cassini interplanetary data has not hitherto been presented, and is the central purpose of the present paper. Here it is shown that by chance all of the HST imaging intervals except that on 13 Jan 2001 correspond to solar wind rarefaction conditions. This allows a comparison of the auroral morphology between a number of images obtained over a one-month interval under these known expanded magnetosphere conditions. The single set of images obtained on 13 Jan 2001 during a compression region are then examined and compared with the images obtained during rarefactions. It is shown that the main oval is brightened over the whole of its observed extent, but that its position is essentially unchanged with respect to the position during rarefaction conditions. However, the auroral region is effectively expanded significantly poleward in the dusk sector by bright contiguous auroras in the 'active region'. We further show that these brightened images were obtained during strongly-varying solar wind conditions within the compression event, involving a modest compression of the magnetosphere followed by a strong and continuous expansion, driven by changes in the solar wind density.

2. Interplanetary data

In this section we discuss the interplanetary data obtained by Cassini during the 2000-2001 fly-by of Jupiter, which provides the context for the HST images. We consider data from the magnetic field instrument MAG [*Dougherty et al.*, 2004] and the CAPS plasma instrument [*Young et al.,* 2004], along with UVIS observations of UV aurora [*Esposito et al.,* 2004]. As an introduction to the data, and to provide a suitable background to this investigation, in Figure 1 we show data from days 275-342 of 2000, i.e. that studied by *Pryor et al.* [2005] which immediately precedes the fly-by interval covered by the HST campaign. From top to bottom the panels show (a) the magnitude of the component of the IMF perpendicular to the radial vector (i.e. perpendicular to the solar wind flow), $B_\perp$ in nT, given in RTN coordinates by $B_\perp = \sqrt{B_T^2 + B_N^2}$, (b) the clock angle of the IMF relative to Jupiter's dipole axis θ in degrees, where each point is spread into a vertical bar

representing the variation in the dipole axis direction over one jovian day (for further details see *Nichols et al.* [2006]), (c) the bulk velocity of the solar wind plasma v_{sw} in km s^{-1}, (d) the number density of the solar wind plasma n_{sw} in cm^{-3}, (e) the dynamic pressure of the solar wind p_{dyn} in nPa, given by $p_{dyn} = \rho v_{sw}^{\,2}$, where ρ is the solar wind plasma mass density calculated from n_{sw} by multiplication with the mean solar wind particle mass (1.92×10^{-27} kg), (f) the estimated jovian subsolar magnetopause standoff distance R_{mp} in R_J (where R_J is Jupiter's radius = 71,373 km), calculated using *Huddleston et al.'s* [1998] empirical formula given by $R_{mp} = 35.5/p_{dyn}(\text{nPa})^{0.22}$ R_J, (g) the integrated auroral power *P* in units of 10^{10} W observed by UVIS (see *Pryor et al.* [2005] for further information), and finally (h) the jovian low-latitude dayside reconnection voltage, estimated using the *Nichols et al.* [2006] algorithm, given by $\phi = v_{sw}B_{\perp}L_o\cos^4(\theta/2)$, where L_o is the width of the channel in the solar wind that reconnects at the magnetopause for exactly northward IMF, taken to be half the subsolar magnetopause standoff distance. All of these data are averaged over ten minute intervals, and gaps in the CAPS data have been linearly interpolated between in the determination of the dayside reconnection voltage.

The abscissa of Figure 1 is labelled with day numbers and the corresponding local time (LT) and radial distance (R_J) of Cassini with respect to Jupiter. It should be noted, however, that all data except that from UVIS are plotted versus estimated time of impact on Jupiter's ionosphere, not at the time of measurement. The time lags of the interplanetary data were computed using the *Khan and Cowley* [1999] method adapted to Jupiter, now briefly detailed. In deriving the solar wind propagation delay, three time periods are considered. These are the solar wind transport time from the point of observation to the subsolar bow shock, the traversal time of plasma through the magnetosheath, and finally the propagation time of solar wind-induced disturbances along magnetospheric field lines to the ionosphere via Alfvén waves. The solar wind transit time is given simply by the solar wind velocity multiplied by the distance along the Sun-planet line between the position of the observed IMF phase front, calculated from Cassini's position by assuming a Parker spiral angle of 11°, and the bow shock position estimated using *Huddleston et al.'s* [1998] empirical formula, given by $R_{BS} = 42.5/p_{dyn}$ (nPa)$^{0.25}$ R_J. The magnetosheath traversal time is then calculated assuming a linear decrease in plasma velocity between that just downstream of the bow shock to that just upstream of the magnetopause. The magnetosonic Mach number for the jovian bow shock is given by *Slavin et al.* [1985] to be ~10, such that we take the velocity just downstream of the bow shock to be $0.26\,v_{sw}$, a value calculated using the usual shock jump conditions for a monatomic plasma. The velocity just upstream of the magnetopause is taken simply to be 30 km s^{-1}, a value

which yields appropriate reconnection voltages of a few hundred kV for low dynamic pressure and a few MV for high dynamic pressure. Finally, the travel time between the magnetopause and the ionosphere is given by one quarter of the period of the fundamental mode eigenoscillations of the outer dayside field lines. Here we employ *Cowley and Bunce's* [2003b] estimation of this propagation time, given by $26\left(R_{mp}\left(\mathrm{R_J}\right)/20\right)^{2.7}$ s. The resulting propagation delays vary from about +55 h at the start of the interval shown in Figure 1, to about +15 h at the end. The photon travel time from Jupiter to Cassini during this interval was less than a minute, such that it can be neglected for purposes of comparison of the UVIS data with the interplanetary data.

It can be seen that the conditions in the interplanetary medium shown in Figure 1 indicate a complex mixture of CIR/CMEs and large amplitude stream interactions, typical of solar maximum. The overall structure, however, is one of sequential intervals of high magnetic field strength (up to ~4 nT) and high dynamic pressure (up to ~1 nPa), followed by several day rarefaction intervals of low magnetic field strength (a few tenths of a nT) and low dynamic pressure (a few hundredths of a nPa). The prevailing clock angles are ±90° and typically change from one to the other during the heliospheric current sheet crossings associated with the CIRs. The estimated reconnection voltage values exhibit a background of order ~100 kV, punctuated by periods of enhanced voltage up to ~3 MV, associated with CIR/CMEs and high strength and/or northward IMF. These values are typical of those found previously by *Nichols et al.* [2006]. The auroral power output also exhibits several major enhancements embedded within the regular ~10 h modulation associated with Jupiter's rotation, specifically on days 280, 292, 295, 309, and 326, as marked by the vertical dashed lines, where the power increases by factors of 2-4. As indicated previously by *Gurnett et al.* [2002] and *Pryor et al.* [2005], these brightenings correspond remarkably well with the compression regions of high magnetic field strength and high reconnection voltage. It is important to emphasise, however, that these brightenings are transient in nature, occurring over time scales of several hours, each one lasting for less than one period of the background modulation associated with Jupiter's rotation. They thus last for periods much shorter than the several day intervals of the compression regions as a whole. The implication is that these major brightenings are thus associated with some specific feature of the compression region events, not with the compression region events as a whole. Judging from the relative timings seen in Figure 1, the brightenings appear to be associated with a central region of the compression events, or even with the trailing edges, rather than with the initial shock-associated compression. However, the few-hour uncertainties in the propagation delay do not allow us to make a more precise statement than this. The UVIS integrated power measurements also do not tell us which component of the aurora is

brightening. With this in mind we now examine the interplanetary conditions associated with the resolved HST UV images obtained during the contiguous fly-by interval.

The trajectory of Cassini during the HST campaign interval is shown in Figure 2. The view is down onto the equatorial plane from the north, with the Sun to the left. The trajectory data are colour-coded according to the physical regime observed, such that red represents the solar wind, blue the magnetosheath, and green the magnetosphere. As an aid to the eye, *Huddleston et al.* [1998] models of the bow shock (blue dot-dashed lines) and magnetopause (green dot-dashed lines) are also shown. The outermost pair of boundaries has been scaled such that the model magnetopause just encompasses the green interval, and corresponds to an expanded state with a low solar wind dynamic pressure of 0.018 nPa. We also note that with this value of the dynamic pressure the model bow shock intersects the spacecraft trajectory where the first bow shock crossing was observed by Cassini. The innermost pair has been scaled such that the bow shock grazes the innermost observed solar wind-magnetosheath transitions, and corresponds to a compressed state with a dynamic pressure of 0.112 nPa. The pattern of bow shock crossings observed by Cassini, indicated by the red-blue trajectory transitions, is thus indicative of strongly-varying system size during the fly-by. The stars with the date labels plotted on the trajectory indicate the times when HST images were obtained.

The interplanetary data obtained by Cassini over the fly-by interval from day 343 of 2000 to day 25 of 2001 are shown in Figure 3, this being contiguous to the interval shown in Figure 1. Again, the data are plotted versus the estimated time of impact on Jupiter's ionosphere, with the propagation delays now ranging from about +15 h at the start of the interval, through zero near closest approach on day 365 of 2000, to about -7 h at the end. The format is also similar to Figure 1, except that integral UV power values from UVIS are no longer available. The field and plasma data are colour coded as in Figure 2, such that solar wind data are red, magnetosheath data are blue, and magnetosphere data are green. Subsolar magnetopause radius estimates and reconnection voltages are shown only when the spacecraft was in the solar wind and relevant data are available, and clock angle values are omitted when the spacecraft was in the magnetosphere. The vertical dashed lines then indicate the times of HST imaging intervals, in which the ~40 min photon travel time from Jupiter to Earth has been taken into account. The associated HST day numbers are shown at the top of the plot for further easy reference.

It can be seen that the first three sets of HST images, obtained on days 349, 351, and 353 of 2000 (14, 16, and 18 Dec), all correspond to a solar wind rarefaction region which followed a high-field

compression region observed between days 343 and 347. During these imaging intervals the solar wind speed was ~450 km s^{-1}, while the density varied between ~0.03 and ~0.1 cm^{-3}, such that the dynamic pressure varied between ~0.01 and ~0.05 nPa. Minimum density and dynamic pressure values occurred for the central image set on day 351, following which there was a small velocity and density increase and a change in IMF polarity prior to the image set on day 353. Estimated subsolar magnetopause radii lie between ~70 and ~100 R_J, thus corresponding to a continuously expanded magnetosphere. Estimated reconnection voltages peak at up to ~500 kV during the first interval, fall to ~100 kV in the second, and increase again to ~500 kV in the third due to a short-lived northward turning of the IMF.

Cassini plasma data are unavailable for the following ~2 week period spanning the fourth HST imaging interval, but the magnetic field observations indicate the presence of a compression region and IMF polarity change between days 355 and 358, with images being obtained on day 363 of 2000 (28 Dec) in the rarefaction region that followed, shortly before the first bow shock crossing was observed by Cassini. The location of the bow shock crossing implies a solar wind dynamic pressure of ~0.018 nPa, with a corresponding expanded subsolar magnetopause distance of ~100 R_J. Conditions were thus likely to have been similar to those occurring in the first three intervals. Following the fourth imaging interval, Cassini crossed the bow shock a number of times between days 364 of 2000 and day 3 of 2001, indicative of significant variations in system size, before briefly encountering the dusk flank magnetosphere itself during days 9-10 of 2001, indicative of a highly expanded system and low solar wind dynamic pressure (of order 0.01 nPa as indicated above) at that time. After this the solar wind dynamic pressure must have increased significantly, since the spacecraft then exited the magnetosphere into the magnetosheath at the end of day 10, and then entered the solar wind early on day 12, where the dynamic pressure and field strength were ~0.1-0.2 nPa and ~0.5-1.5 nT respectively. The corresponding estimated subsolar magnetopause radius was ~50-60 R_J. The fifth HST image set, obtained on day 13 of 2001 (13 Jan), thus corresponds to a magnetosphere that was significantly more compressed than the first four, and had been so for at least two days previously. The estimated reconnection voltage during the interval peaked at ~1 MV. Overall, this solar wind compression region lasted until day 18, after which the spacecraft re-entered the magnetosheath due to a drop in dynamic pressure and although the remaining data were thus obtained in the magnetosheath it is clear that the IMF strength fell once more to small values. The sixth and seventh HST imaging intervals on days 20 and 21 of 2001 thus again correspond to solar wind rarefaction conditions.

In summary, it can thus be seen that six out of the seven HST imaging intervals were obtained during conditions of low solar wind dynamic pressure and IMF field strength at Jupiter, when the magnetosphere is expected to have been considerably expanded (to ~70-100 R_J at the subsolar magnetopause), and the magnetopause reconnection rate was very low (at most a few 100 kV). This, nevertheless, affords the opportunity of comparing auroral morphologies in a number of cases of known similar interplanetary conditions, obtained over a period of about six weeks. We note that these images were obtained at intervals from ~2 days after the end of the previous magnetospheric compression (days 349 of 2000 and 20 of 2001) to ~6 days after (day 353 of 2000). Only one imaging interval during the campaign was obtained under conditions of some compression, on day 13 of 2001, where the estimated magnetopause position was typically ~50-60 R_J, and the magnetopause reconnection rate peaked at ~1 MV. This case therefore merits special consideration and comparison with the other images obtained during the campaign.

3. HST observations

Due to the asymmetric nature of Jupiter's internal planetary field, a more complete view of the jovian auroras can be obtained from Earth for the northern hemisphere than for the southern. Consequently we here focus exclusively on the northern auroras. Even so, good viewing is limited to less than a half of Jupiter's rotation period, when the planetary dipole axis, which is offset from the planetary rotation axis by ~9.5°, is tilted towards the Earth. Correspondingly, northern images were obtained during the Cassini campaign only between ~110° and ~300° central meridian longitude (CML), where the CML is the System III (SIII) longitude at the centre of the planet facing the observer. In fact the images obtained cluster in two CML ranges in which the overall viewing is favourable, ~160° to ~180°, and ~210° to ~230° (see e.g. Figures 7 of *Grodent et al.* [2003a,b]). For ease of direct comparison, here we therefore compare selected images obtained during the various imaging intervals which are close to the centre of these two CML ranges. Images within the ~160° to ~180° CML range were obtained in six of the seven intervals, the exception being the fifth (compression region) interval on day 13 of 2001. All of these images thus correspond to solar wind rarefaction conditions and an expanded magnetosphere. They will be briefly compared with each other in the following sub-section in order to form a well-defined baseline for comparison with the compression region images. Images within the ~210° to ~230° CML range were also obtained in six of the seven intervals, the exception now being the fourth

interval on day 363 of 2001. These images therefore correspond to five cases of solar wind rarefaction conditions and one of compression, and will be discussed thereafter.

3.1 Comparison of images with CML in the range ~160° to ~180°

Representative examples from each of the six intervals for which images were obtained in the CML range from ~160° to ~180° are shown in Figure 4, all of which correspond to solar wind rarefaction conditions as discussed above. The images have been projected onto a jovigraphic latitude-longitude grid looking down onto the north pole, with the CML directed towards the bottom of each image, such that dawn is to the left and dusk to the right. Latitude and longitude lines are shown by the grey dashed lines at intervals of 10° each, and longitude increases clockwise around the plots. The stretching of the auroral features towards the top of the images results from their location near the planet's limb as viewed by the HST, such that these features should be treated with caution. Further details of the projection are provided by *Grodent et al.* [2003b]. The images have been plotted using a logarithmic intensity scale saturated at 250 kR, such that the fainter polar auroras can be observed as well as the brighter main oval emissions. The red dashed lines show the reference main oval determined by *Grodent et al.* [2003b] from the full Cassini campaign data set.

It can first be seen that the main oval presents similar features in all six images, lying closely along the reference main oval in each case. As usual, a narrow smooth oval is present at SIII longitudes between ~240° and ~160°, which lies in the dawn to noon sector for this CML range. At smaller SIII longitudes, here lying on the dusk side, the oval is broader, though generally brightest at its poleward border, and exhibits a marked 'kinked' appearance, as described previously by *Grodent et al.* [2003b]. In Figure 5a we show the maximum auroral intensity along the narrow smooth part of the main oval for each of these images, plotted versus SIII longitude between 240° in the dawn sector and 160° near noon. Generally the intensity is similar in each image, lying typically in the range ~100-200 kR, but exhibits peaks up to ~400-600 kR. The peaks in the noon sector are typically narrow in longitude and vary significantly from image to image, while all images except for that obtained on day 351 of 2000 exhibit a broad peak centred near SIII longitude ~220° in the dawn sector. The intensity along the thickened kinked part of the oval cannot conveniently be plotted versus SIII longitude since it lies almost along a fixed SIII meridian at ~150°. Consequently in Figure 5b we instead plot it versus latitude between ~55° and ~80°, where the values given correspond to the maximum values observed near to the reference oval at the poleward edge of the

distribution. In this case the luminosities are typically somewhat larger than in the narrow smooth part of the oval, being ~200-300 kR, but again having peaks of ~400-500 kR. Overall, however, although the intensity distribution around the main oval does vary somewhat from image to image, as can be seen in Figures 4 and 5, its principal features remain essentially fixed over the whole image set.

The 'polar auroras' located within the main oval show much greater variability. As discussed previously by *Grodent et al.* [2003a], two principal components may be identified. The first occurs within the central part of the polar region and consists of numerous patchy forms, whose intensity typically lies between a few tens of kR and ~100 kR. This has been termed the 'swirl' region by *Grodent et al.* [2003a], and appears to be co-located with the 'fixed dark polar region' (f-DPR) observed by *Stallard et al.* [2003] in H_3^+ infrared emissions. This region has been interpreted to correspond to the near-stagnant region of open field lines mapping to the tail [*Cowley et al.,* 2003*; Grodent et al.,* 2003a]. Often the patches are arranged to form a diffuse ring with a central darker region, examples of which can be seen in the images on days 349, 351, 353 and possibly 363 of 2000 in Figure 4. 'Reduced ovals' of this nature inside the main oval have been discussed previously by *Prangé et al.* [1998] and *Pallier and Prangé* [2001]. This morphology is then reminiscent of the two-ring auroral structure obtained in the axi-symmetric jovian flow and current models presented by *Cowley et al.* [2005]. In these models the outer ring (the main oval) maps to the corotation breakdown region of the middle magnetosphere at equatorial radial distances of ~20-40 R_J, while the inner ring surrounds the region of open field lines. Sometimes, however, the polar auroral patches appear to more uniformly cover the central region, as occurs on days 20 and 21 of 2001.

The second component of the polar auroras then occurs in the band between the central region of patchy 'swirl' auroras and the main oval, which on the basis of the above discussion is suggested to map to the further regions of the equatorial magnetosphere, beyond ~40 R_J. In the dawn sector this region is invariably devoid of auroral forms at intensities above a few tens of kR. In the post-noon and dusk sector, however, the region contains highly variable forms that *Grodent et al.* [2003a] term the 'active region'. The brightest such aurora in Figure 4 is that observed on day 349 of 2000 (Figure 4a), where the intensity peaks at ~650 kR. Bright auroras throughout this region are also observed on day 20 of 2001 (Figure 4e), with a distinctive bright spot peaking at ~300 kR occurring near noon, and to some extent also on day 21 of 2001. It is then interesting to note that these cases all occurred shortly (~2-3 days) after the end of major compressions of the magnetosphere by the solar wind (Figure 3). On the other hand, only weak emissions are observed in the dusk sector in

this region on days 351 and 353 of 2000, such that in these cases the central region of patchy auroras is surrounded by a dark region at all local times that are visible. These images were obtained ~4-6 days after a major compression. There is thus some suggestion in these data that the occurrence or otherwise of bright auroras in the active sector might relate to time since a major magnetospheric compression. However, a moderate display in this region with intensities peaking at ~250 kR is also present on day 363 of 2000 (Figure 4d). Although no solar wind plasma data are available during this period, the IMF data in Figure 3 indicate that this interval occurred at least ~3 days following a compression. The suggestion of an association of bright 'active region' auroras with intervals following compression regions is thus interesting, but is not conclusive from this data set.

We also note that no clear correspondence is evident between either of the polar auroral components and the estimated magnetopause reconnection voltage shown in Figure 3. As indicated in section 2 above, the estimated voltages were very low indeed (~100 kV) on days 351 and 363 of 2000, and also presumably on days 20 and 21 of 2001, while being modestly enhanced (~500 kV) on days 349 and 353. However, no systematic differences in the aurora between these images (e.g. the presence or absence of 'noon spots' that might correspond to the dayside cusp) are evident in Figure 4. It should be recognised, however, that all of these voltages are relatively small in terms of flux transport in the jovian magnetosphere.

3.2 Comparison of images with CML in the range ~210° to ~230°

We now turn to the images obtained in the second CML range, and in Figure 6 similarly show six selected images obtained with the CML close to ~220°. Five of them were obtained during the same imaging intervals as were shown in Figure 4, taken typically ~1.5 h after the latter during the same jovian rotation. These are the images shown for days 349, 351, and 353 of 2000 (Figures 6a-c), and for days 20 and 21 of 2001 (Figures 6e-f), all of which are thus similarly associated with solar wind rarefaction region conditions. Images in this CML range were not obtained on day 363 of 2000, as shown in Figure 4d, and are replaced in Figure 6d by an image obtained on day 13 of 2001 (correspondingly not available at CML ~170°), which we recall is the sole HST interval representative of solar wind compression region conditions.

If we first compare the rarefaction region images between Figures 4 and 6 it can be seen that the overall auroral morphology remains very similar between each pair of corresponding images,

though due to the rotation of the planet the visible part of the main oval now corresponds principally to the narrow smooth part, while the broader kinked part is generally close to the dusk limb and appears distorted in the projected images. Apart from this effect, however, the main oval again lies close to the rotated reference oval in each case, with the slight displacements observed in e.g. in Figure 6e being due to projection uncertainties associated with the determination of the position of the centre of the planet. The peak brightness along the narrow smooth oval is plotted versus SIII longitude in Figure 7, in the same format as Figure 5a. Each rarefaction region image now shows peaks of ~400-800 kR at the dusk end (SIII ~180° to ~160°), before falling to ~100-200 kR at earlier local times. On days 20 and 21 there are also peaks of ~500-700 kR at dawn (SIII ~220° to ~240°). Although the general pattern of intensity variation along the narrow smooth main oval thus differs somewhat between Figures 4 and 6, the typical and peak values are similar in both cases. The polar auroras are also similar in corresponding cases. In particular, patchy inner rings continue to be observed in the central region on days 349, 351, and 353 of 2000, while more general patchy forms are present on days 20 and 21 of 2001. Corresponding 'active region' auroras also continue in the post-noon sector on day 349 of 2000, where they now take the form of a ~300 kR arc lying between the central patchy auroras and the main oval which merges with the latter in the dusk sector, and on days 20 and 21 of 2001, where the emission is more diffuse as it had been earlier. Overall, therefore, the rarefaction region images in Figure 6 retain the basic features discussed above in relation to Figure 4.

We thus now consider the compression region image obtained on day 13 of 2001 shown in Figure 6d. First, we see that the main oval continues to be located close to the reference oval over the range of SIII longitudes that this can be accurately determined, its deviation being not further than e.g. in Figure 6e mentioned above. However, it is brightened considerably along its whole length compared with all the other images. As can be seen in Figure 7d, the typical brightness varies between ~300 and ~500 kR, with peaks up to ~1 MR. While the main oval is still relatively narrow in the dawn sector, in the post-noon sector it appears in essence to merge with bright active region auroras to produce a continuous but variable band of bright forms extending poleward of the usual main oval position by up to ~5° of latitude. The intensity within this band is ~200-400 kR. The morphology observed in this image thus lends support to the association between bright active region auroras and solar wind compressions suggested above, at least to the extent that such auroras can clearly be excited during such intervals. Inside the main/active region oval, patchy auroral forms now fill almost the whole of the polar region, though with the suggestion of a lessening in intensity at dawn in a narrow region adjacent to the main oval. The intensity of this mottled aurora peaks at ~100 kR. Overall, this image shows that all components of the aurora are significantly

affected by the changed solar wind conditions, exhibiting significant enhancements in either brightness or extent.

Two images were in fact obtained near the above CML range on day 13 of 2001, the one shown in Figure 6d at CML 219°, and a second observed ~40 min later at CML 242°. In Figure 8 we show both of these images due to their unusual nature, but now with a revised colour scale which allows the brightness variations along the main oval and in the active region to be resolved. Both images show a bright main oval lying essentially along the usual reference oval in the dawn sector, giving way to more patchy intensifications along the reference oval at dusk. A continuous but variable band of emission then extends poleward of the main oval in the dusk sector, corresponding to the active region, which is even brighter in the second image than in the first. These auroras peak at ~700 kR in the second image, and form a somewhat irregular secondary arc lying just poleward of the main oval at dusk, rather reminiscent of the active region arc seen on day 349 of 2000 shown in Figure 6a, which was observed ~2 days following the end of a compression region. These images thus show that the form of the brightened main oval persisted on this day for an interval of at least ~1 h.

The simplest interpretation of these brightened images is that they are representative of a modified auroral morphology occurring under conditions in which the jovian magnetosphere is relatively compressed by the solar wind, contrary to the theoretical expectations of *Southwood and Kivelson* [2001] and *Cowley and Bunce* [2001, 2003a,b]. However, we noted above in relation to Figure 1 that the enhancements in integrated UV power observed by UVIS are transient in nature, lasting typically for less than one jovian rotation (i.e. of order a few hours). Consequently, they must correspond to some specific feature of the compression region events, rather than to the events as a whole. If the brightened oval observed by the HST on day 13 of 2001 is then related to the UVIS brightenings, as seems entirely probable given the magnitude of the emission enhancements, it seems plausible that they may also represent a transient state which is not necessarily representative of the compression region as a whole. In this case it is important to examine the concurrent solar wind conditions in more detail.

In Figure 9 we thus show Cassini solar wind data (red) spanning the interval of the two images shown in Figure 8 (vertical dashed lines) on an expanded time-base from 1200 on day 12 of 2001 to 0100 on day 14. The format is the same as for Figure 3, but with an increased magnetic field resolution of 1 min. The solar wind propagation delays during the interval are typically ~-1 h, now computed using an assumed Parker spiral phase front of 8.5°, tailored to the low solar wind speeds

observed during the interval. The uncertainty in the lag propagation delays are also estimated to be about ±4 h, based on a study of how the values depend upon the assumed parameters employed, as outlined in Section 2 above. Based on these uncertainties, our best estimate of the solar wind interval which pertains to the two brightened HST images is that contained between the two grey vertical dashed lines in Figure 9, with the timing of the two images using the nominal propagation delay being shown by the two vertical black lines. The apparent 'back-tracking' of the Cassini data in this interval (and others) is a consequence of the variable lag times derived as the interplanetary parameters vary, and is indicative of rapidly-changing conditions. This artefact and the initial data gap notwithstanding, it can be seen that the two brightened images correspond to very dynamic solar wind conditions within the compression region event. The magnetopause first compressed inward from ~55 to ~45 R_J due to a rapid increase in solar wind density, following which an extended interval of magnetospheric expansion took place from ~45 to ~80R_J over ~9 h due to continuously falling solar wind density. The spacecraft then exited the solar wind into the correspondingly expanded magnetosheath (see Figure 3). Within the present uncertainties we do not know in detail how the images relate to these variations. We would point out, however, that they are not necessarily in conflict with the theoretical picture presented by *Southwood and Kivelson* [2001] and *Cowley and Bunce* [2001, 2003a,b] in which brightened main ovals are associated with intervals containing strong magnetospheric expansion. Clearly, imaging and interplanetary data of greater coverage and temporal resolution are required to further pursue this important issue. We should also comment that given the restricted nature of the present data set, it also not possible to identify specific auroral features that might be associated with the simultaneously elevated magnetopause reconnection rates.

4. Summary & discussion

In this paper we have provided a detailed discussion of the relation between the extensive set of jovian UV auroral images observed by HST-STIS in Dec 2000–Jan 2001 and the simultaneous interplanetary data obtained in situ by Cassini during its Jupiter fly-by. We showed that by chance six of the seven HST observation intervals correspond to solar wind rarefactions (dynamic pressures of a few times 0.01 nPa) which follow compressions by intervals of between ~2 and ~6 days. Only the images obtained on day 13 of 2001 correspond compression region conditions (dynamic pressures of generally a few times 0.1 nPa, but highly variable).

We first examined the auroral morphology corresponding to rarefaction regions, which acts as a benchmark against which the compression region images can be compared. It is found that these images exhibit a relatively restricted range of behaviours, with the main oval auroras consistently located close to the previously-determined reference oval, and with intensities typically in the range ~100-300 kR. Small-scale patchy auroras with intensities peaking at ~100 kR then occupy the central part of the polar region, often forming a diffuse central ring with a dark interior, while on other occasions being more uniformly distributed. The region between the patchy central auroras and the main oval is invariably dark in the dawn and pre-noon sector, while being intermittently filled with bright auroras in the post-noon and dusk sector, termed the 'active region'. On occasion the auroras in the latter region form bright diffuse and arc-like structures which fill the region between the patchy central auroras and the main oval. On other occasions the auroral emission in the 'active' region is weak, such that in these cases the central patchy region is surrounded by a dark band at all local times that are visible in the images. There is some suggestion that bright active region auroras may be associated particularly with rarefaction region images obtained within ~2-3 days of compressions, and that these may largely disappear after ~4-6 days, though the present data set is not conclusive on this point. In addition, no clear association between the auroral distribution and the estimated magnetopause reconnection rate has been found in these data, though the latter is relatively small in all these cases, at most a few hundred kV.

We then examined the images obtained for day 13 of 2001 at CML 219° and 242°, during a compression region in which the dynamic pressure of the solar wind and IMF strength were generally significantly increased, but nevertheless highly variable. Major changes were observed in all the auroral components, well removed from the range of behaviours observed in the set of rarefaction region images. The main oval was significantly brighter over almost the whole length observed, with typical intensities of ~300-500 kR, peaking at ~1 MR. The position of the oval, however, was essentially unchanged relative to the reference oval within the uncertainties. Contiguous bright 'active region' forms with intensities ~200-700 kR were also present in the post-noon and dusk sector, which in effect widened the overall auroral distribution in this sector by up to ~5° in the poleward direction. Patchy auroras peaking at ~100 kR were also observed over almost the whole of the central polar region down to the main oval/active region, though with the suggestion of a much-narrowed darker zone just poleward of the main oval in the dawn and pre-noon sector. Overall, therefore, remarkably different auroral properties are observed in this interval compared with the full set of rarefaction region images.

With only two images available to illustrate auroral properties under these compression region conditions, and with little indication of auroral evolution and time scales, it seems somewhat premature to attempt an extended physical interpretation of these results. However, a few comments are appropriate. First, with regard to the 'swirl' region of patchy auroras, if these correspond to the region of open field lines, as surmised above, then the expansion in the region of these forms observed in the compression region images perhaps indicates a growth in the amount of open flux in the system. This would not be unexpected given the elevated IMF strengths and increased dayside magnetopause reconnection rates characteristic of such intervals [*Nichols et al.,* 2006]. However, the detailed mechanism leading to the formation of such patchy auroras on open field lines remains completely unknown at present. In addition, given the two compression region images available, it is not possible to discriminate possible auroral features associated specifically with the expected elevated magnetopause reconnection rates, such as those associated with the cusp.

With regard to the observations of the main oval, the nature of our conclusions depend strongly on whether we take the images to be representative of the compression region as a whole, or to reflect more transient conditions within the compression region. If they are representative of compression regions as a whole, then clearly they confound reasonable initial theoretical expectation that the intensity of the main oval should anti-correlate with the solar wind dynamic pressure [*Southwood and Kivelson,* 2001; *Cowley and Bunce,* 2001, 2003a,b]. A caveat to this statement occurs if the compression is so severe that the plasma is brought to a state of super-rotation with respect to the neutral atmosphere [*Cowley and Bunce,* 2003a,b], an effect that could be enhanced by atmospheric inertia [*Gong and Hill,* 2005]. In this case the corotation enforcement current system will be reversed in sense, such that while the usual region of the main oval will be aurorally dark, associated with a downward-directed field-aligned current, a bright aurora associated with upward field-aligned current could occur in the poleward region. However, we do not believe this to be the origin of the bright main oval discussed here for two reasons. First, there is no evidence that the brightened oval examined here is systematically shifted poleward of its usual location. Rather, it continues to be located along the main reference oval defined by *Grodent et al* [2003b]. Second, the images were obtained at least two days after the onset of the compression, over which time scale transient plasma super-rotation should not be expected to persist [*Cowley and Bunce,* 2003a,b].

It should also be recognised, however, that solar wind compression regions contain significant sub-structure which might relate to the auroral brightening. In this context we emphasise that the integrated UV brightenings reported in UVIS data by *Gurnett et al.* [2002] and *Pryor et al.* [2005]

615 are transient in nature, lasting for few-hour intervals which are much shorter than the compression regions as a whole. On the reasonable assumption that the brightened ovals observed here may be physically related to the UVIS events, and thus also transient in nature, we have therefore examined the related interplanetary data observed by Cassini at high time resolution. We have found that the brightened images correspond to an interval of strongly varying solar wind conditions and
620 consequent magnetospheric dynamics, in which the magnetosphere undergoes a modest compression followed by an extended major expansion. We are not able to say exactly which feature the images correspond to within the timing uncertainties, but can conclude that they are not necessarily in conflict with the theoretical picture presented by *Southwood and Kivelson* [2001] and *Cowley and Bunce* [2001, 2003a,b] in which brightenings are associated with magnetospheric
625 expansion. Imaging and interplanetary data with greater temporal resolution are required to further address these issues.

Acknowledgements

JDN and SWHC were supported during the course of this study by PPARC grant PPA/G/O/2003/00013, while EJB was supported by a PPARC Postdoctoral Fellowship. The authors wish to thank Prof Michele Dougherty and Dr Nick Achilleos at Imperial College London for provision of Cassini MAG and trajectory data, Dr Abi Rymer at John Hopkins University for Cassini boundary crossing data, and Dr Frank Crary at the Southwest Research Institute for the CAPS data. CAPS is supported by a contract with NASA/JPL. JDN wishes to thank Dr Steve Milan for helpful discussions.

References

Achilleos, N., M.K. Dougherty, D.T. Young, and F.J. Crary (2004), Magnetic signatures of Jupiter's bow shock during the Cassini fly-by, J. Geophys. Res., 109, A09S04, doi:10.1029/2003JA010258.

Alexeev, I.I. and E.S. Belenkaya (2005), Modeling of the jovian magnetosphere, Ann. Geophysicae, 23, 809-826.

Baron, R., T. Owen, J.E.P. Connerney, T. Satoh, and J. Harrington (1996), Solar wind control of Jupiter's H_3^+ auroras, Icarus, 120, 437-442.

Bunce, E.J., S.W.H. Cowley, and T.K. Yeoman (2004), Jovian cusp processes: Implications for the polar aurora, J. Geophys. Res., 109, A09S13, doi:10.1029/2003JA010280.

Clarke, J.T., G. Ballester, J. Trauger, J. Ajello, W. Pryor, K. Tobiska, J.E.P Connerney, G.R. Gladstone, J.H. Waite Jr., L.B. Jaffel, and J.–C. Gérard (1998), Hubble Space Telescope imaging of Jupiter's UV aurora during the Galileo orbiter mission, J. Geophys. Res., 103(E9), 20217-20236, doi: 10.1029/98JE01130.

Cowley, S.W.H. and E.J. Bunce (2001), Origin of the main auroral oval in Jupiter's coupled magnetosphere-ionosphere system, Planet. Space Sci., 49, 1067-1088.

Cowley, S.W.H. and E.J. Bunce (2003a), Modulation of jovian middle magnetosphere currents and auroral precipitation by solar wind-induced compressions and expansions of the magnetosphere: Initial conditions and steady state, Planet. Space Sci., 51, 31-56.

Cowley, S.W.H. and E.J. Bunce (2003b), Modulation of Jupiter's main auroral oval emissions by solar wind induced expansions and compressions of the magnetosphere, Planet. Space Sc. 51, 57-79.

Cowley, S.W.H., E.J. Bunce, T.S. Stallard, and S. Miller (2003), Jupiter's polar ionospheric flows: theoretical interpretation, Geophys. Res. Lett., 30(5), 1220, doi:10.1029/2002GL016030.

Cowley, S.W.H., I.I. Alexeev, E.S. Belenkaya, E.J. Bunce, C.E. Cottis, V.V. Kalegaev, J.D. Nichols, R. Prangé, and F.J. Wilson (2005), A simple axisymmetric model of magnetosphere-ionosphere coupling currents in Jupiter's polar ionosphere, J. Geophys. Res., 110, A11209, doi:10.1029/2005JA011237.

Dougherty, M.K., S. Kellock, D.J. Southwood, A. Balogh, E.J. Smith, B.T. Tsurutani, B. Gerlach, K.-H. Glassmeier, F. Gleim, C.T. Russell, G. Erdos, F.M. Neubauer, and S.W.H. Cowley (2004), The Cassini magnetic field investigation, Space Sci. Rev., 114, 331-383.

Elsner, R.F., N. Lugaz, J.H. Waite Jr., T.E. Cravens, G.R. Gladstone, P. Ford, D. Grodent, A. Bhardwarj, R.J. MacDowall, M.D. Desch, and T. Majeed (2005), Simultaneous Chandra X ray, Hubble Space Telescope ultraviolet, and Ulysses radio observations of Jupiter's aurora, J. Geophys. Res., 110, A01207, doi:10.1029/2004JA010717.

Esposito, L.W., C.A. Barth, J.E. Colwell, G.M. Lawrence, W.E. McClintock, A.I.F. Stewart, H.U. Keller, A. Korth, H. Lauche, M.C. Festou, A.L. Lane, C.J. Hansen, J.N. Maki, R.A. West, H. Jahn, R. Reulke, K. Warlich, D.E. Shemansky, and Y.L. Yung (2004), The Cassini ultraviolet imaging spectrograph investigation, Space Sci. Rev., 115, 294–361.

Gong, B. and T.W. Hill (2005), Variations of Jovian and Saturnian auroras induced by changes of solar wind dynamic pressure, Magnetospheres of the Outer Planets 2005 Programme and Abstracts, p. 129, University of Leicester, Leicester, UK.

Grodent, D., J.T. Clarke, J.H. Waite Jr., S.W.H. Cowley, J.-C. Gérard, and J. Kim (2003a), Jupiter's polar auroral emissions, J. Geophys. Res., 108(A10), 1366, doi:10.1029/2003JA010017.

Grodent, D., J.T. Clarke, J. Kim, J.H. Waite Jr, and S.W.H. Cowley (2003b), Jupiter's main oval observed with HST-STIS, J. Geophys. Res., 108(A11), 1389, doi:10.1029/2003JA009921.

Grodent, D., J.-C. Gérard, J.T. Clarke, G.R. Gladstone, and J.H. Waite Jr. (2004), A possible auroral signature of a magnetotail reconnection process on Jupiter, J. Geophys. Res., 109, A05201, doi:10.1029/2003JA010341.

Gurnett, D.A., W.S. Kurth, G.B. Hospodarsky, A.M. Persoon, P. Zarka, A. Lecacheux, S.J. Bolton, M.D. Desch, W.M. Farrell, M.L. Kaiser, H.P. Ladreiter, H.O. Rucker, P. Galopeau, P. Louarn, D.T. Young, W.R. Pryor, and M.K. Dougherty (2002), Control of Jupiter's radio emission and aurorae by the solar wind, Nature, 415 (6875), 985-987.

Hanlon P.G., M.K. Dougherty, R.J. Forsyth, M.J. Owens, K.C. Hansen, G. Tóth, F.J. Crary, and D.T. Young (2004), On the evolution of the solar wind between 1 and 5 AU at the time of the Cassini Jupiter fly-by: Multi-spacecraft observations of interplanetary coronal mass ejections including the formation of a merged interaction region, J. Geophys. Res., 109, A09S03, doi:10.1029/2003JA010112.

Hanlon P.G., M.K. Dougherty, N. Krupp, K.C. Hansen, F.J. Crary, D.T. Young, and G. Tóth (2004), Dual spacecraft observations of a compression event within the Jovian magnetosphere: Signatures of externally triggered supercorotation?, J. Geophys. Res., 109, A09S09, doi:10.1029/2003JA010116.

Hill, T.W. (2001), The jovian auroral oval, J. Geophys. Res., 106, 8101-8108.

Huddleston, D.E., C.T. Russell, M.G. Kivelson, K.K. Khurana, and L. Bennett (1998), Location and shape of the jovian magnetopause and bow shock, J. Geophys. Res., 103, 20075-20082.

Khan, H. and S.W.H. Cowley (1999), Observations of the response time of high-latitude ionospheric convection to variations in the interplanetary magnetic field using EISCAT and IMP-8 data, Ann. Geophysicae, 17, 1306-1335.

Nichols, J.D. and S.W.H. Cowley (2004), Magnetosphere-ionosphere coupling currents in Jupiter's middle magnetosphere: Effect of precipitation-induced enhancements of the Pedersen conductivity, Ann. Geophysicae, 22, 1799-1827.

Nichols, J.D. , S.W.H. Cowley, and D.J. McComas (2006), Magnetopause reconnection rate estimates for Jupiter's magnetosphere based on interplanetary measurements at ~5AU, Ann. Geophysicae, 24, 393–406.

Pallier, L. and R. Prangé (2001), More about the structure of the high latitude jovian aurorae, Planet. Space Sci., 49, 1159-1173, doi:10.1016/S0032-0633(01)00023-X.

Prangé, R., D. Rego, L. Pallier, J.E.P. Connerney, P. Zarka, and J. Queinnec (1998), Detailed study of FUV jovian auroral features with the post-COSTAR HST faint object camera, J. Geophys. Res., 103(E3), 20195-20216, doi: 10.1029/98JE01128.

Pryor, W.R., A.I.F. Stewart, L.W. Esposito, W.E. McClintock, J.E. Colwell, A.J. Jouchoux, A.J. Steffl, D.E. Shemansky, J.M. Ajello, R.A. West, C.J. Hansen, B.T. Tsurutani, W.S. Kurth, G.B. Hospodarsky, D.A. Gurnett, K.C. Hansen, J.H. Waite, F.J. Crary, D.T. Young, N. Krupp, J.T. Clarke, D. Grodent, and M.K. Dougherty (2005), Cassini UVIS observations of Jupiter's auroral variability, Icarus, 178, 312-326.

Slavin, J.A., E.J. Smith, J.R. Spreiter, and S.S. Stahara (1985), Solar wind flow about the outer planets: Gas dynamic modeling of the Jupiter and Saturn bow shocks, J. Geophys. Res., 90, 6275-6286.

Southwood, D.J. and M.G. Kivelson (2001), A new perspective concerning the influence of the solar wind on Jupiter, J. Geophys. Res., 106, 6123-6130.

Stallard T.S., S. Miller, S.W.H. Cowley, and E.J. Bunce (2003), Jupiter's polar ionospheric flows: Measured intensity and velocity variations poleward of the main auroral oval, Geophys. Res. Lett., 30 (5), 1221, doi:10.1029/2002GL016031.

Svenes, K.R., B.T. Narheim, A.J. Coates, D.R. Linder, and D.T. Young (2004), Cassini Plasma Spectrometer electron measurements close to the magnetopause of Jupiter, J. Geophys. Res., 109, A09S06, doi:10.1029/2003JA010254.

Waite Jr., J.H., G.R. Gladstone, W.S. Lewis, R. Goldstein, D.J. McComas, P. Riley, R.J. Walker, P. Robertson, S. Desai, J.T. Clarke, and D.T. Young (2001), An auroral flare at Jupiter, Nature, 410, 787-789.

Young, D.T., J.J. Berthelier, M. Blanc, J.L. Burch, A.J. Coates, R. Goldstein, M. Grande, T.W. Hill, R.E. Johnson, V. Kelha, D.J. McComas, E.C. Sittler, K.R. Svenes, K. Szego, P. Tanskanen, K. Ahola, D. Anderson, S. Bakshi, R.A. Baragiola, L. Barraclough, R.K. Black, S. Bolton, T. Booker, R. Bowman, P. Casey, F.J. Crary, D. Delapp, G. Dirks, N. Eaker, H. Funsten, J.D. Furman, J.T. Gosling, H. Hannula, C. Holmlund, H. Huomo, J.M. Illiano, P. Jensen, M.A.

775 Johnson, D.R. Linder, T. Luntama, S. Maurice, K.P. McCabe, K. Mursula, B.T. Narheim, J.E. Nordholt, A. Preece, J. Rudzki, A. Ruitberg, K. Smith, S. Szalai, M.F. Thomsen, K. Viherkanto, J. Vilppola, T. Vollmer, T.E. Wahl, M. Wuest, T. Ylikorpi, and C. Zinsmeyer (2004), Cassini plasma spectrometer investigation, Space Sci. Rev., 114, 1-112.

Figure Captions

Figure 1. Plot showing the conditions in the interplanetary medium as measured by Cassini over days 275-343 of 2000. From top to bottom the panels show: the perpendicular IMF magnitude $B_{\perp}$ in nT, the IMF clock angle relative to Jupiter's spin axis θ in degrees, the velocity of the solar wind v_{sw} in km s^{-1}, the number density of the solar wind n_{sw} in cm^{-3} on a log scale, the dynamic pressure of the solar wind p_{dyn} in nPa on a log scale , the estimated jovian subsolar magnetosphere radius R_{mp} in R_J, the total integrated UV auroral power as observed by UVIS, and the estimated reconnection voltage ϕ in kV, as described in the text. Data are plotted versus estimated time of impact on Jupiter's ionosphere, along with the local time and range of Cassini relative to Jupiter. In the plots for θ and ϕ each 'data point' is stretched into a vertical line representing the effect produced by the ~±9.5° diurnal variation of Jupiter's dipole axis offset. The dashed grey lines indicate the times of enhanced auroral power output as observed by UVIS.

Figure 2. Plot showing the trajectory of Cassini in the planet's equatorial plane during the Jupiter fly-by interval from 343/2000 to 025/2001. The view is down from the north with the Sun to the left, and the colour scheme is such that solar wind intervals are red, magnetosheath intervals are blue and magnetosphere intervals are green. Slavin et al. (1985) models of the bow shock and magnetopause are shown by the blue and green dot-dashed lines, respectively, for dynamic pressures of 0.0072 nPa and 0.125 nPa. The stars with day labels show when the HST images were obtained.

Figure 3. As Figure 1, but for the period of the HST campaign, i.e days 343/2000 to 025/2001. No integrated UVIS data are available for this interval. The pairs of dashed vertical grey lines bracket the times of emission of the auroral photons observed by HST for those images considered here, i.e. with CML greater than 100° and less than 250°. The data colour scheme is the same as for Figure 2, i.e. solar wind is red, magnetosheath blue, and magnetosphere green.

Figure 4. Images of Jupiter's northern UV aurora with CML ~160°-180° obtained by the HST during the millennium campaign, projected onto a latitude-longitude grid viewed from above the north pole. The CML of each image, i.e. approximately the sunward direction, is aligned toward the bottom of each image, such that dawn is to the left, dusk to the right, and midnight to the top. The intensity scale is logarithmic and saturated at 250 kR. The *Grodent et al.* [2003b] reference main oval is shown by the dashed red line. A $10^{o} \times 10^{o}$ jovigraphic grid is overlaid. The images

were obtained on (a) 349/2000, (b) 351/2000, (c) 353/2000, (d) 363/2000, (e) 020/2001, and (f) 021/2001.

Figure 5. Plots of the peak auroral brightness along the main oval plotted as a function of (a) longitude in the 'narrow arc' region between 160° and 240° and (b) latitude in the kinked more diffuse auroral region between 56° and 82°. The horizontal dashed line denotes 250 kR, i.e. the value at which the images in Figure 4 are saturated. The longitude scale in (a) is reversed in sense in order to link intuitively with the clockwise-increasing longitude values in Figure 4. The order of the panels is the same as that for the images in Figure 4.

Figure 6. As Figure 4, but for images with CML ~210°-230°. The images were obtained on (a) 349/2000, (b) 351/2000, (c) 353/2000, (d) 013/2001, (e) 020/2001, and (f) 021/2001.

Figure 7. As Figure 5a, but for the images shown in Figure 6.

Figure 8. HST images obtained on 13 January 2001 with CMLs of 219° and 242°. The format is as for Figures 4 and 6, but with the colour scale saturated at 700 kR.

Figure 9. As Figure 3, but for the period from 1200hrs on day 012 of 2001 to the end of day 013, and with an increased MAG data resolution of 1 min.

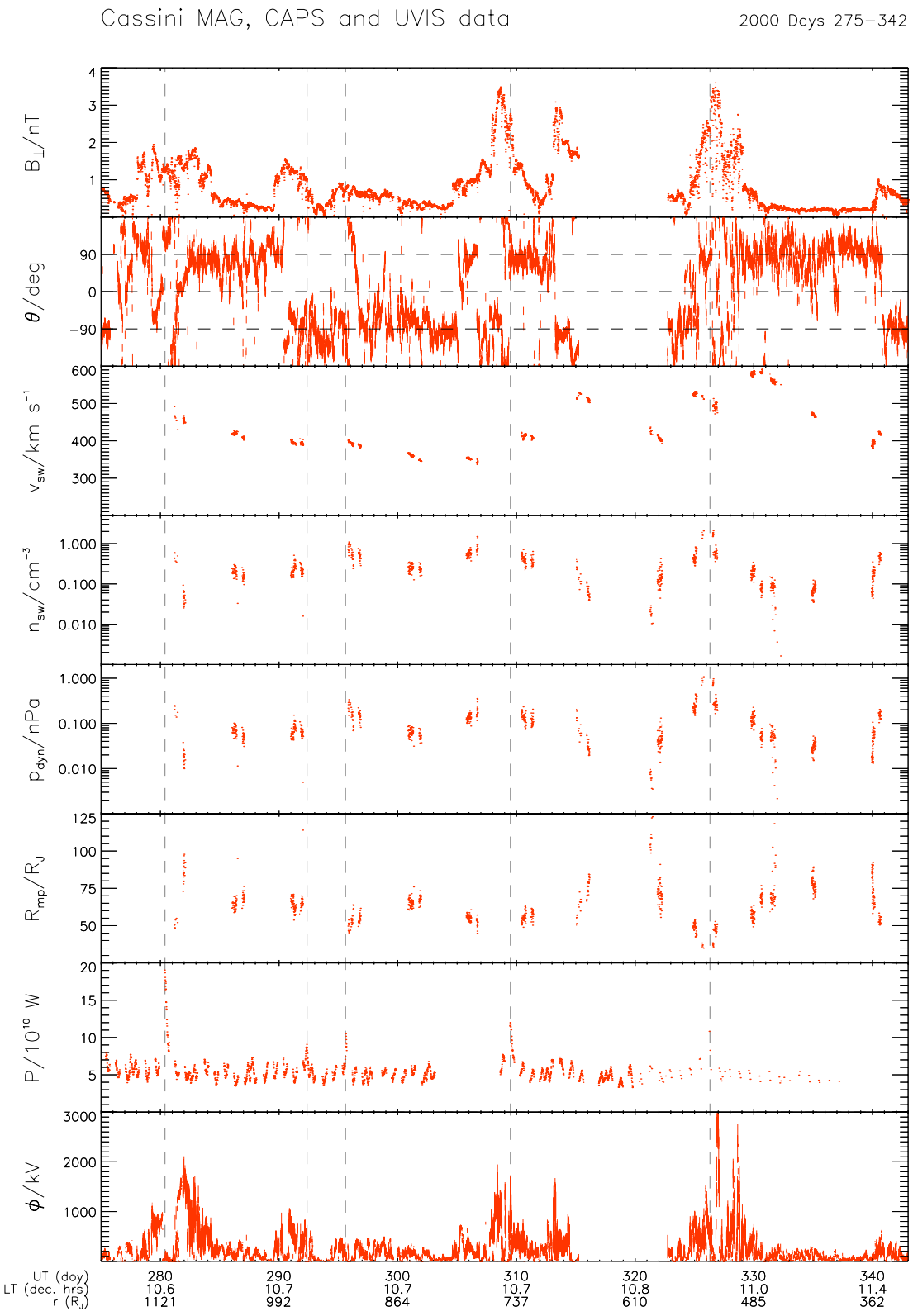
Cassini MAG, CAPS and UVIS data
2000 Days 275–342
B⊥/nT
θ/deg
v_sw/km s^-1
n_sw/cm^-3
p_dyn/nPa
R_mp/R_J
P/10^10 W
φ/kV
UT (doy)
LT (dec. hrs)
r (R_J)
280 290 300 310 320 330 340
10.6 10.7 10.7 10.7 10.8 11.0 11.4
1121 992 864 737 610 485 362

Figure 1

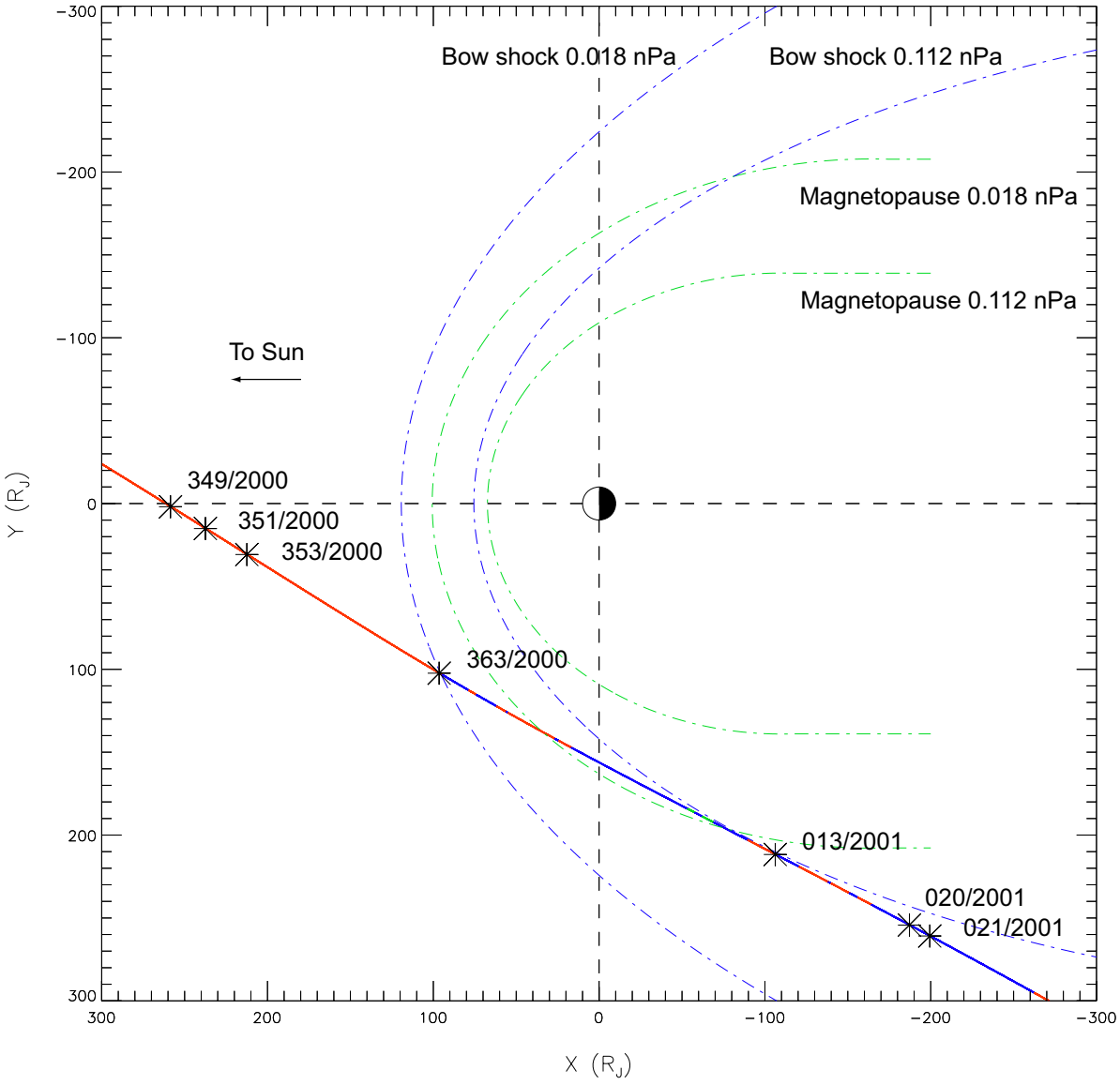
Bow shock 0.018 nPa
Bow shock 0.112 nPa
Magnetopause 0.018 nPa
Magnetopause 0.112 nPa
To Sun
349/2000
351/2000
353/2000
363/2000
013/2001
020/2001
021/2001
Y (R_J)
X (R_J)
300
200
100
0
−100
−200
−300

Figure 2

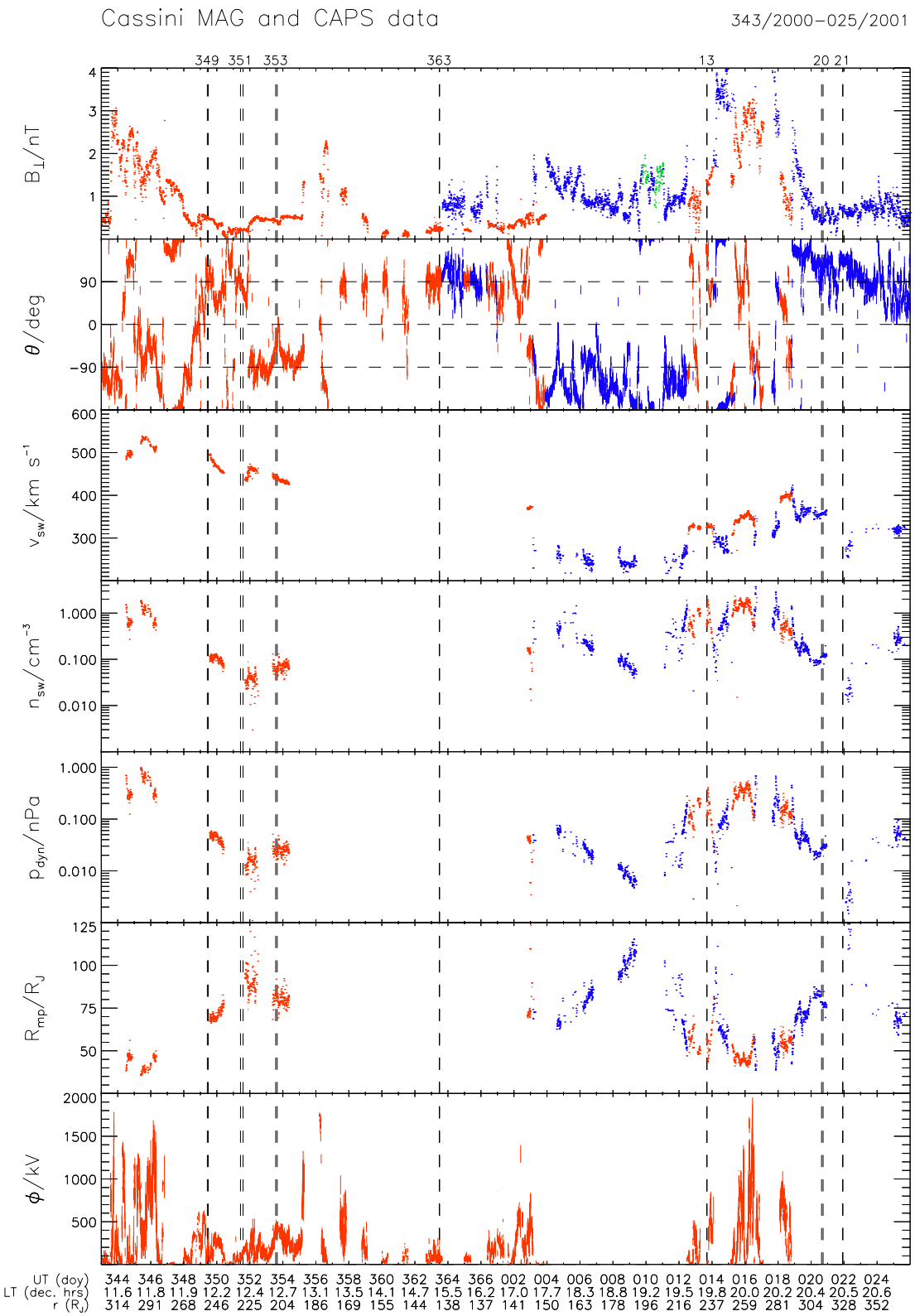
Cassini MAG and CAPS data
343/2000–025/2001
349 351 353 363 13 20 21
B⊥/nT
θ/deg
v_sw/km s^-1
n_sw/cm^-3
p_dyn/nPa
R_mp/R_J
ϕ/kV
UT (doy) 344 346 348 350 352 354 356 358 360 362 364 366 002 004 006 008 010 012 014 016 018 020 022 024
LT (dec. hrs) 11.6 11.8 11.9 12.2 12.4 12.7 13.1 13.5 14.1 14.7 15.5 16.2 17.0 17.7 18.3 18.8 19.2 19.5 19.8 20.0 20.2 20.4 20.5 20.6
r (R_J) 314 291 268 246 225 204 186 169 155 144 138 137 141 150 163 178 196 216 237 259 281 304 328 352

Figure 3

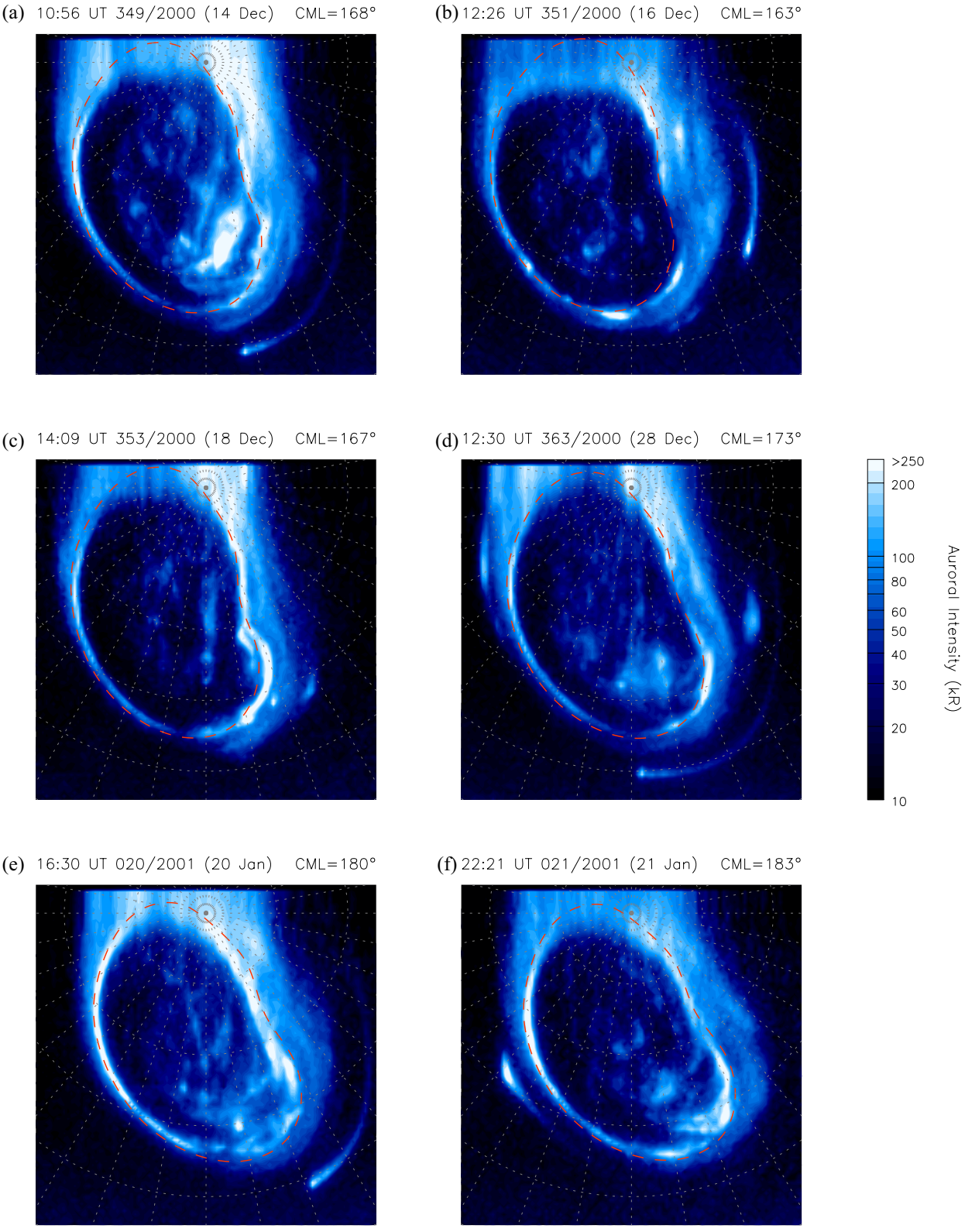
(a) 10:56 UT 349/2000 (14 Dec) CML=168°
(b) 12:26 UT 351/2000 (16 Dec) CML=163°
(c) 14:09 UT 353/2000 (18 Dec) CML=167°
(d) 12:30 UT 363/2000 (28 Dec) CML=173°
(e) 16:30 UT 020/2001 (20 Jan) CML=180°
(f) 22:21 UT 021/2001 (21 Jan) CML=183°
>250
200
100
80
60
50
40
30
20
10
Auroral Intensity (kR)

Figure 4

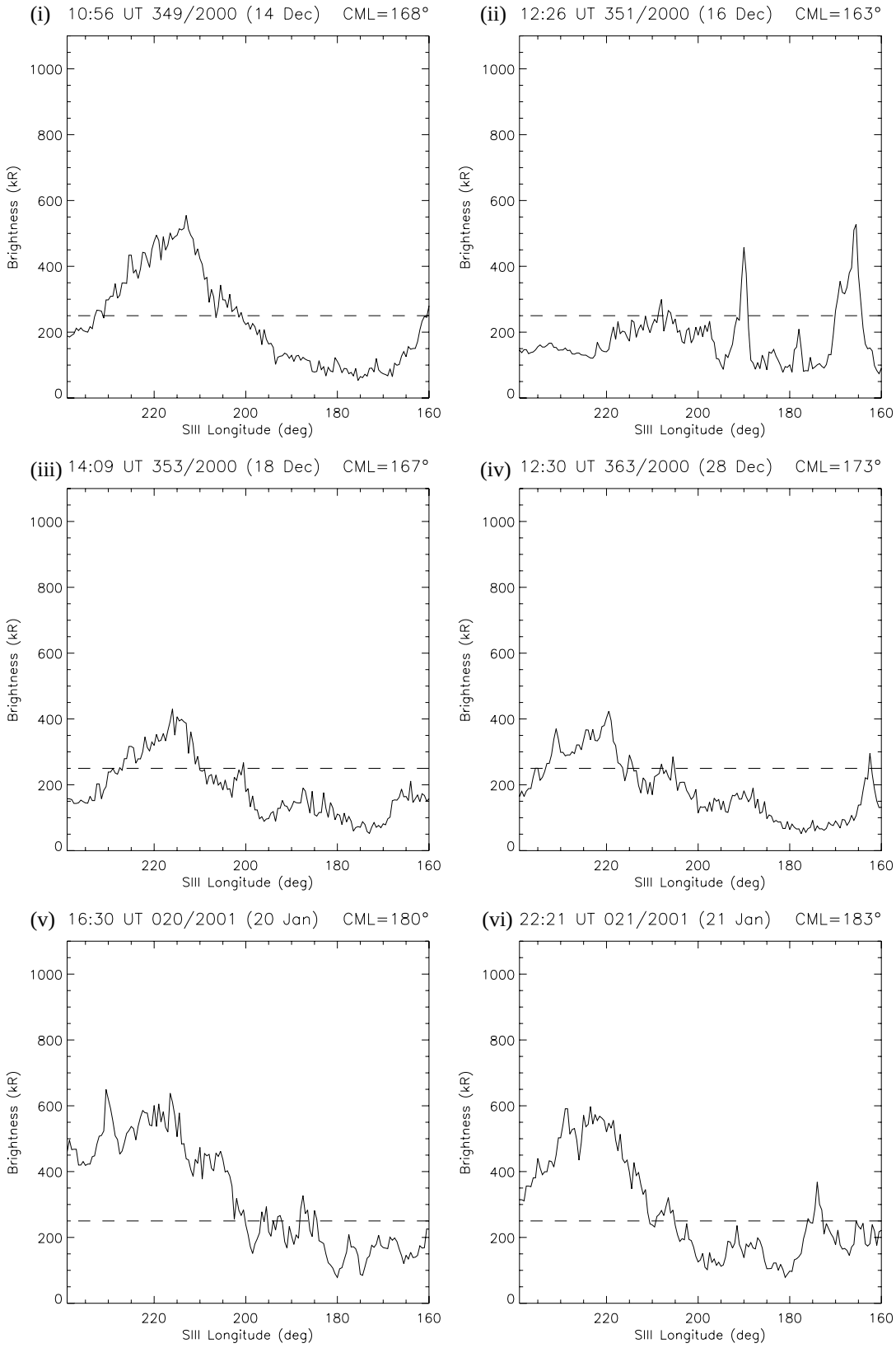
(i) 10:56 UT 349/2000 (14 Dec) CML=168°
(ii) 12:26 UT 351/2000 (16 Dec) CML=163°
(iii) 14:09 UT 353/2000 (18 Dec) CML=167°
(iv) 12:30 UT 363/2000 (28 Dec) CML=173°
(v) 16:30 UT 020/2001 (20 Jan) CML=180°
(vi) 22:21 UT 021/2001 (21 Jan) CML=183°
Brightness (kR)
SIII Longitude (deg)
0
200
400
600
800
1000
220
200
180
160

Figure 5a

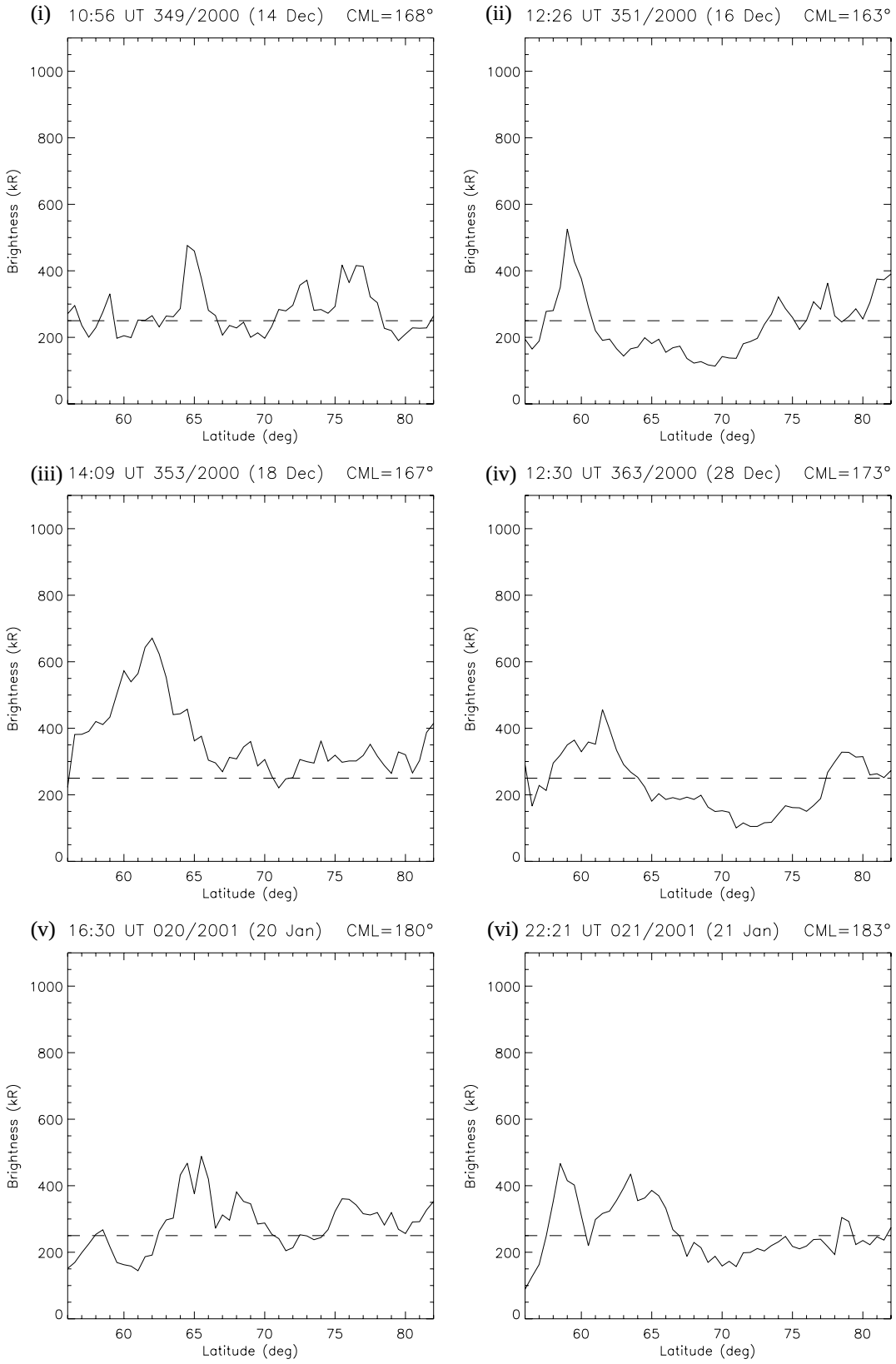
(i) 10:56 UT 349/2000 (14 Dec) CML=168°
(ii) 12:26 UT 351/2000 (16 Dec) CML=163°
(iii) 14:09 UT 353/2000 (18 Dec) CML=167°
(iv) 12:30 UT 363/2000 (28 Dec) CML=173°
(v) 16:30 UT 020/2001 (20 Jan) CML=180°
(vi) 22:21 UT 021/2001 (21 Jan) CML=183°
Brightness (kR)
Latitude (deg)
0
200
400
600
800
1000
60
65
70
75
80

Figure 5b

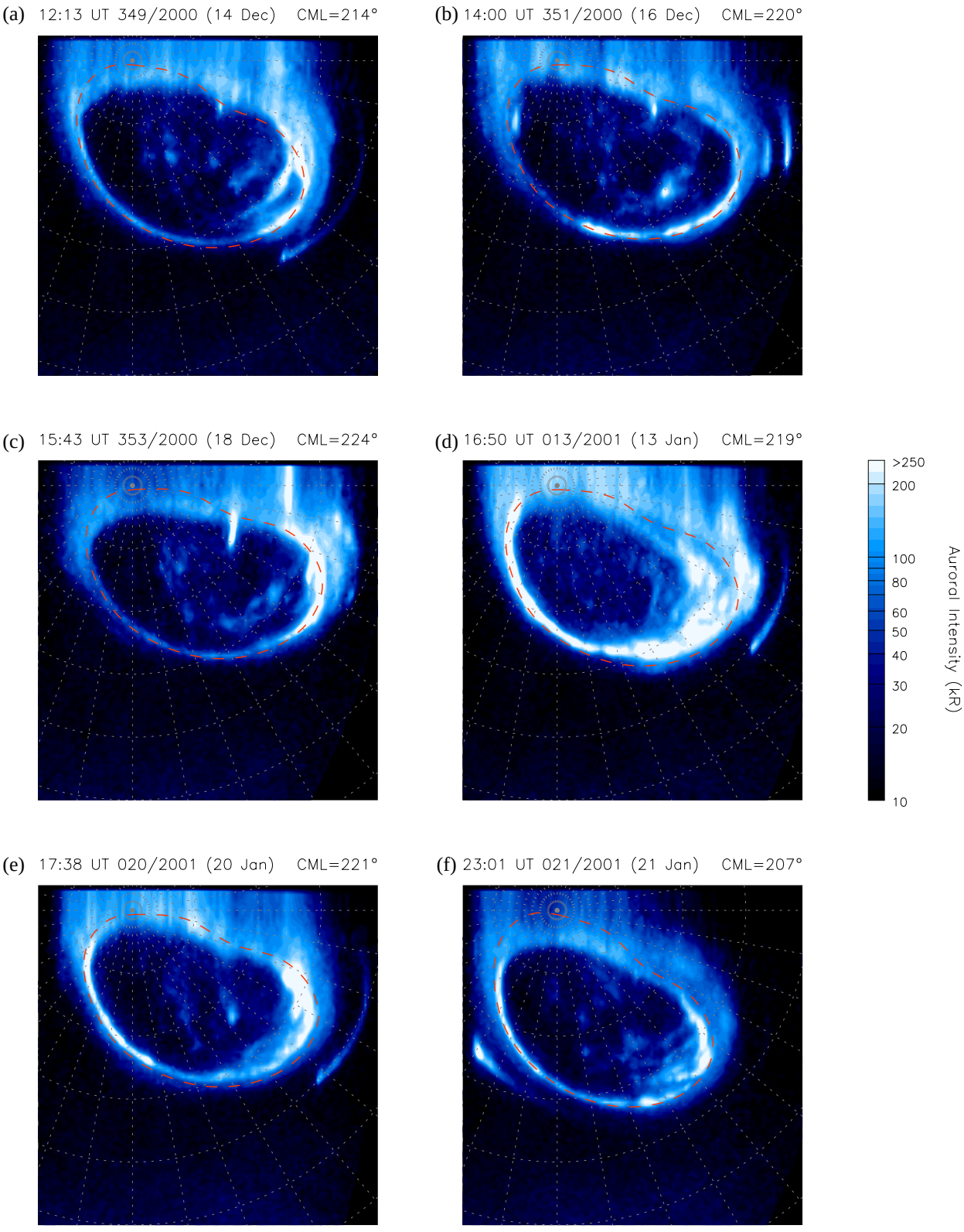
(a) 12:13 UT 349/2000 (14 Dec) CML=214°
(b) 14:00 UT 351/2000 (16 Dec) CML=220°
(c) 15:43 UT 353/2000 (18 Dec) CML=224°
(d) 16:50 UT 013/2001 (13 Jan) CML=219°
(e) 17:38 UT 020/2001 (20 Jan) CML=221°
(f) 23:01 UT 021/2001 (21 Jan) CML=207°
>250
200
100
80
60
50
40
30
20
10
Auroral Intensity (kR)

Figure 6

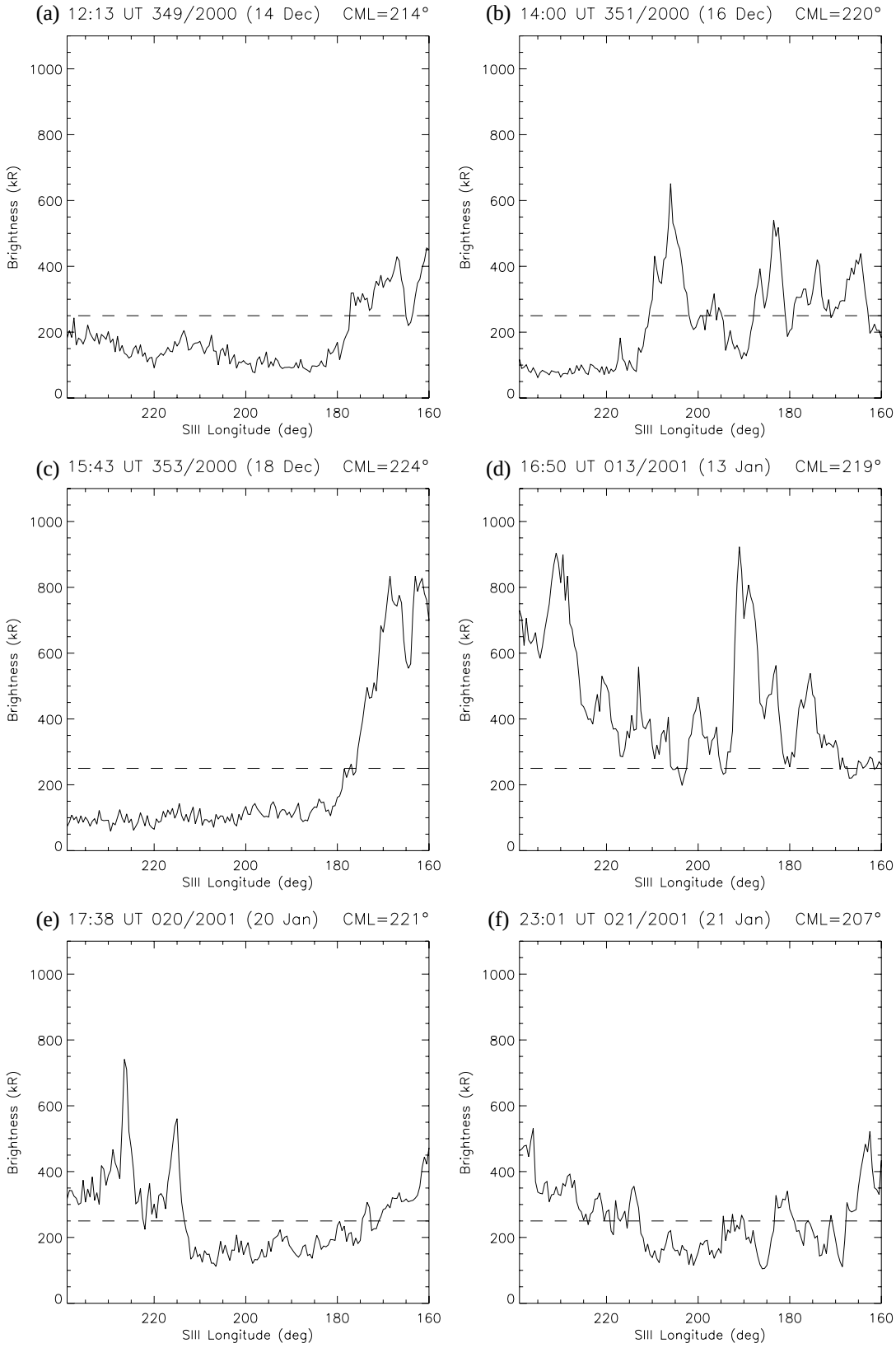
(a) 12:13 UT 349/2000 (14 Dec) CML=214°
(b) 14:00 UT 351/2000 (16 Dec) CML=220°
(c) 15:43 UT 353/2000 (18 Dec) CML=224°
(d) 16:50 UT 013/2001 (13 Jan) CML=219°
(e) 17:38 UT 020/2001 (20 Jan) CML=221°
(f) 23:01 UT 021/2001 (21 Jan) CML=207°
Brightness (kR)
SIII Longitude (deg)
0
200
400
600
800
1000
220
200
180
160

Figure 7

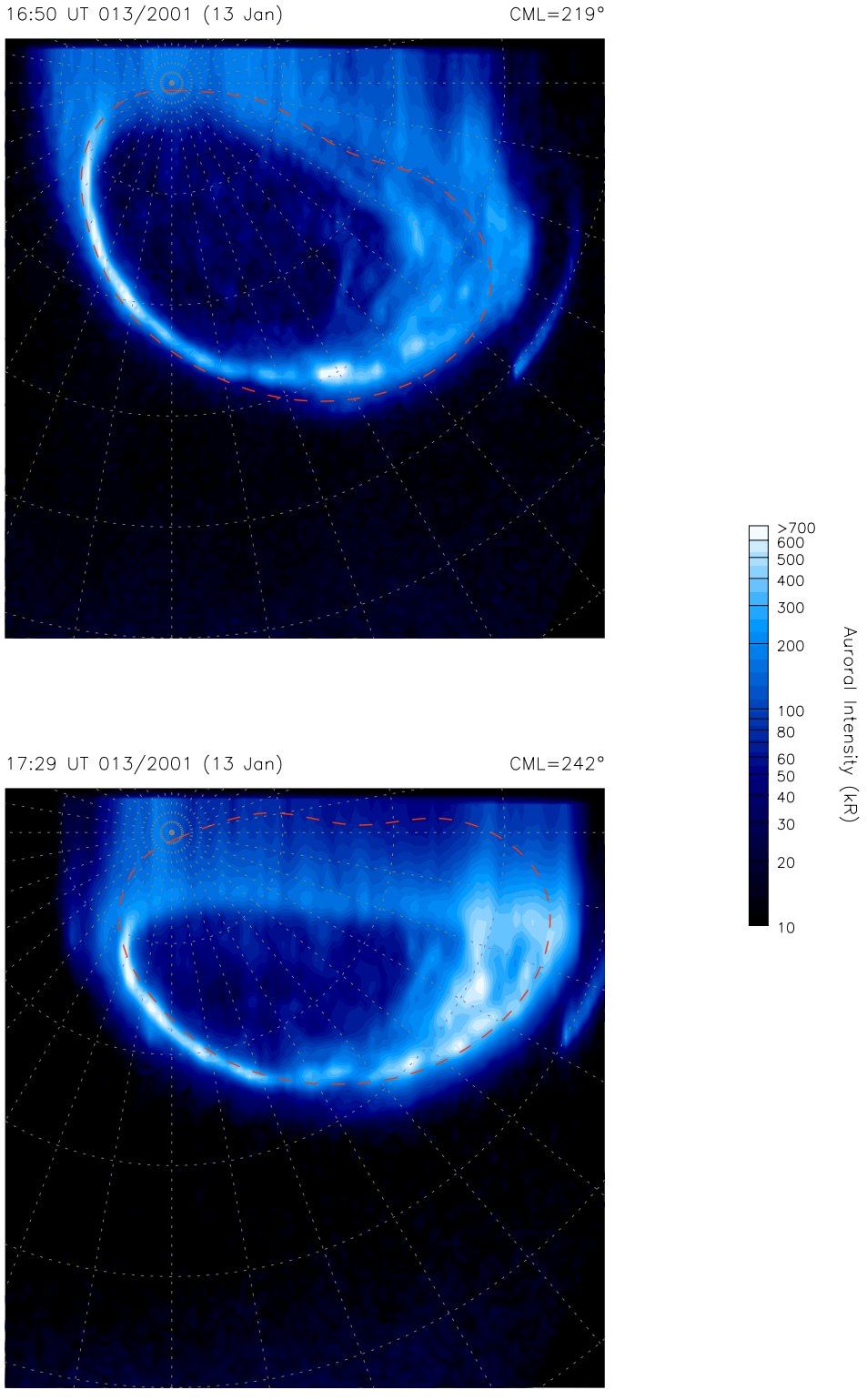
16:50 UT 013/2001 (13 Jan)
CML=219°
17:29 UT 013/2001 (13 Jan)
CML=242°
>700
600
500
400
300
200
100
80
60
50
40
30
20
10
Auroral Intensity (kR)

Figure 8

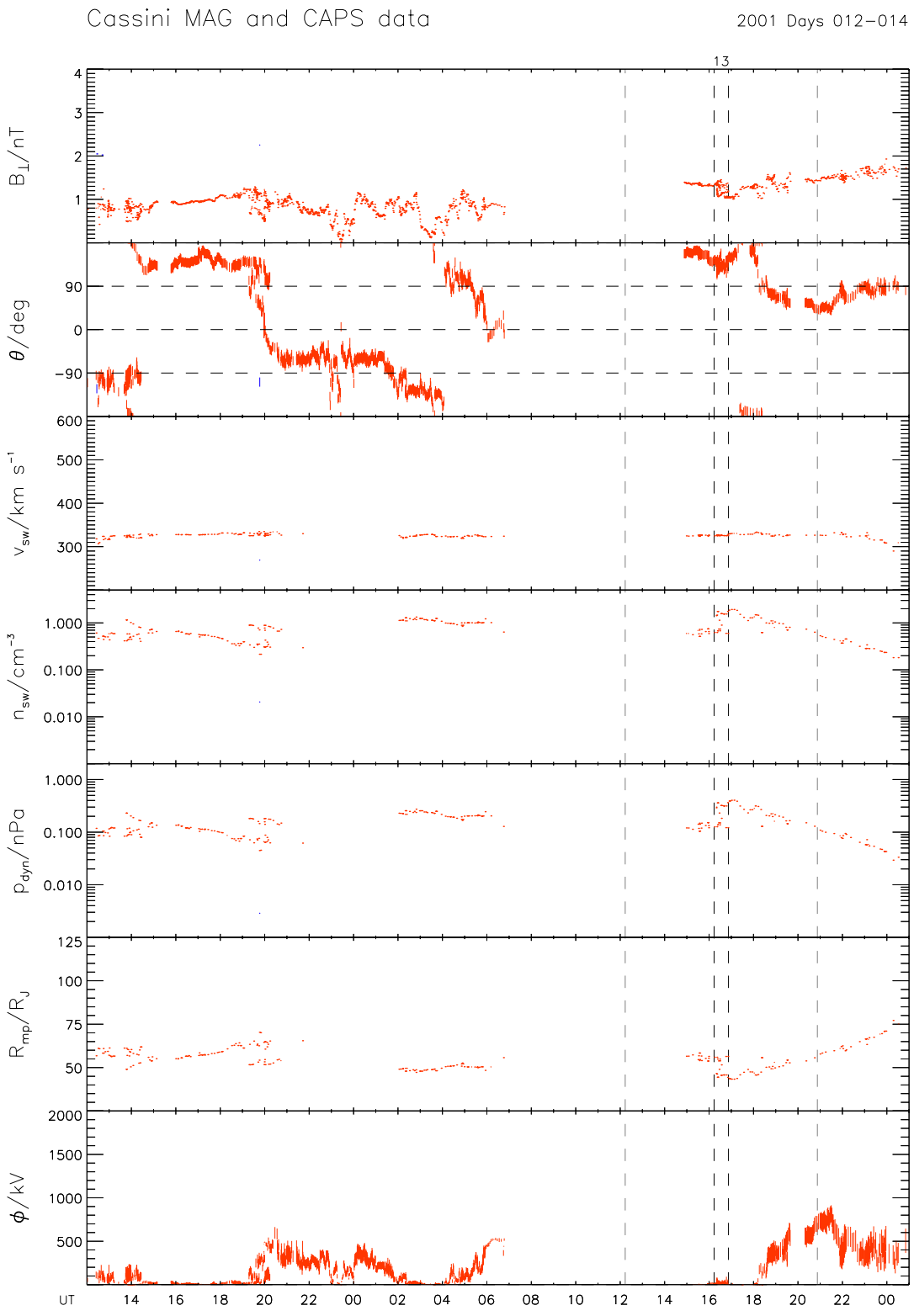
Cassini MAG and CAPS data
2001 Days 012–014
13
B⊥/nT
θ/deg
v_sw/km s^-1
n_sw/cm^-3
p_dyn/nPa
R_mp/R_J
φ/kV
UT
14 16 18 20 22 00 02 04 06 08 10 12 14 16 18 20 22 00

Figure 9